ARTICLE INFO
Article ID: 14-09-02-0010

doi:10.4271/14-09-02-0010

Time-Optimal Coordination Control for the Gear-Shifting Process in Electric-Driven Mechanical Transmission (Dog Clutch) without Impacts

Ziwang Lu,[1] Guangyu Tian,[1] and Simona Onori[2]

[1]Tsinghua University, China
[2]Stanford University, USA

Abstract

Torque interruption and shift jerk are the two main issues that occur during the gear-shifting process of electric-driven mechanical transmission. Herein, a time-optimal coordination control strategy between the the drive motor and the shift motor is proposed to eliminate the impacts between the sleeve and the gear ring. To determine the optimal control law, first, a gear-shifting dynamic model is constructed to capture the drive motor and shift motor dynamics. Next, the time-optimal dual synchronization control for the drive motor and the time-optimal position control for the shift motor are designed. Moreover, a switched control for the shift motor between a bang-off-bang control and a receding horizon control (RHC) law is derived to match the time-optimal dual synchronization control strategy of the drive motor. Finally, two case studies are conducted to validate the bang-off-bang control and RHC. In addition, the method to obtain the appropriate parameters of the drive motor and shift motor is analyzed according to the coordination control method.

History

Received: 20 Feb 2020
Revised: 14 Apr 2020
Accepted: 10 Jun 2020
e-Available: 23 Jun 2020

Keywords

Electric vehicles, Electric-driven mechanical transmission, Gear-shifting process, Time-optimal coordination control

Citation

Lu, Z., Tian, G., and Onori, S., "Time-Optimal Coordination Control for the Gear-Shifting Process in Electric-Driven Mechanical Transmission (Dog Clutch) without Impacts," *SAE Int. J. Elect. Veh.* 9(2):2020, doi:10.4271/14-09-02-0010.

ISSN: 2691-3747
e-ISSN: 2691-3755

1. Introduction

Electric vehicles (EVs) are being pursued as a transportation solution to address current energy and environmental concerns [1]. Adopting transmissions in EVs can not only extend the torque range, but also improve the working point of the drive motor. In addition to automatic transmissions, continuously variable transmissions, and dual-clutch transmissions, automatic mechanical transmissions (AMTs) are also a good option owing to their low price and high efficiency [2, 3]. By using a drive motor, the clutch between the drive motor and the AMT can be removed, thereby reducing both weight and cost of the powertrain. This system is called a clutchless automatic mechanical transmission (CLAMT). However, the torque interruption and the shift jerk would deteriorate the performance of a CLAMT.

This problem can be addressed from two main perspectives. The first focuses on drive motor control, whereas the second focuses on the shift motor control. With respect to the drive motor control, numerous studies have been conducted to investigate the active speed synchronization. Falcone Frank et al. [4] and Junqiang Xi et al. [5] analyzed the effect of the rotational speed difference between the sleeve and the gear ring on the active speed synchronization time. The results demonstrated that the active synchronization time increased, but the impacts will be reduced with the decrease in the terminal speed difference. To pursue a fast and robust control, Hong Fu et al. [6] and Yu et al. [7, 8] applied sliding mode control to adjust the speed of the drive motor. Zhu et al. [9] applied an H_∞ preview control to achieve speed synchronization. In other studies, motor active synchronization control was applied to a hybrid powertrain to compensate for the shortage due to the slow response of the internal combustion engine [10, 11, 12]. Currently, focus is directed toward the CLAMT without a synchronizer, which is called the electric-driven mechanical transmission (EMT). In such a system, only electric motors are involved in the gear-shifting process. Furthermore the optimal final speed difference scale has been investigated in a few studies. Results reveal that the gear-shifting success probability increases with the final speed difference at the same angle difference [13, 14]. Additionally, the dual synchronization of angle and speed has been investigated. Dual synchronization implies synchronizing the speed while aligning the angle difference. In a dual synchronization, no speed difference or angle difference is achieved between the sleeve and gear ring. Hence, the impacts between the two components disappear. To save dual synchronization time, Piracha et al. [15] proposed a rule-based dual synchronization control through the analysis of pure speed synchronization, whereas Lu et al. [16] obtained the theoretical solution for a time-optimal dual synchronization control based on Pontryagin's minimum principle (PMP).

The gear-shifting actuator is crucial in the gear shifting process. In comparison with hydromechanical actuators, electromechanical actuators are a better option as they are lightweight and easy to control [17]. A study that mainly focused on the fast position control to reduce the duration of torque interruption was conducted. Zhong et al. [18, 19] directly replaced a shift lever with a shift motor and proposed a time-optimal control combining bang-bang control and a linear quadratic regulator (LQR). An LQR is used at the last stage to reduce the magnitude of the solution overshoot. Gao et al. [20] designed a sliding mode control to track the optimal trajectory from an LQR. Chen et al. [21] applied the H_∞ preview control to attain the desired position by considering the future reference curve.

Without using a synchronizer, a time-optimal coordination control law can be applied in the EMT to eliminate the impacts between the sleeve and the gear ring. To obtain the ideal control law, the equations of motion are first achieved. Subsequently, the time-optimal dual synchronization control and position control are achieved for the drive motor and shift motor, respectively. Next, a switched position control for the shift motor between the bang-off-bang control and receding horizon control (RHC) is designed to match the dual synchronization of the drive motor. Finally, two cases i.e., one using bang-off-bang control and the other using RHC, are simulated to validate the algorithm. Moreover, the method to select the parameters of the drive motor and the shift motor considering the control policy is proposed.

2. Mechanical Structure

Figure 1 illustrates the EMT used in this study. The EMT comprises a drive motor, a mechanical transmission, and a gear-shifting actuator. The drive motor is connected to the mechanical transmission directly with no clutch in between. There is also no synchronizer between the sleeve and the gear ring.

The EMT system can be classified into two categories according to the motion, i.e., the gear rings rotationally driven by the drive motor and the sleeve translationally driven by the gear-shifting actuator. The power flow indicated in red represents the rotational motion driven by the drive motor. There are two shifting actuators in Figure 1(b). Each gear-shifting actuator includes a shift motor, planetary reduction mechanism, gear and sector gear mechanism, and shift finger. The rotational motion of the shift motor is first reduced by a planetary gear reducer and a gear and sector gear mechanism; subsequently, it is converted into the translation of the sleeve by the shifting finger pushing the sleeve. Details of the geometry and motion of the gear-shifting actuator are presented in Appendix A. During the gear-shifting process, the sleeve is driven by the shift motor from the original gear to the target gear.

3. Gear-Shifting Process Dynamic Model

A dynamic model was constructed to depict the gear-shifting process is built. Based on the motion sources, the dynamic model can be classified into two categories, i.e., the motion driven by the drive motor and that driven by the shift motor.

FIGURE 1 Mechanical structure of the EMT. The shaded lines indicate the power flows with the first gear.

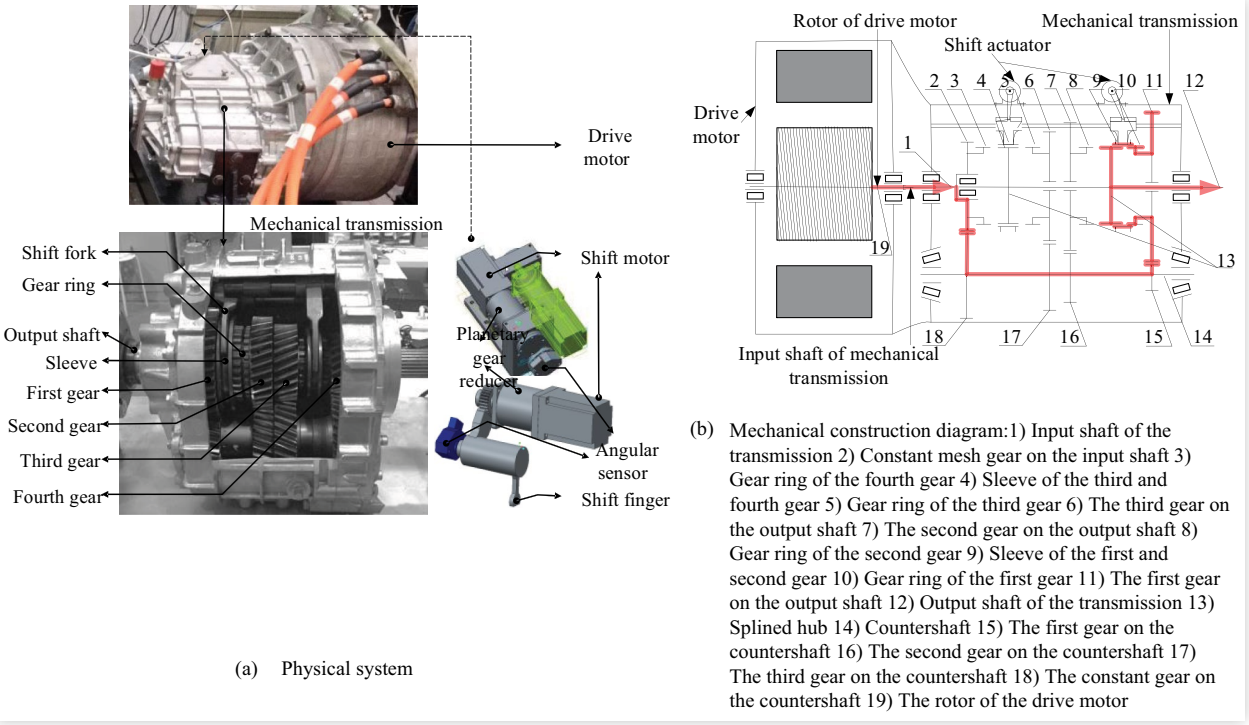

(a) Physical system

(b) Mechanical construction diagram:1) Input shaft of the transmission 2) Constant mesh gear on the input shaft 3) Gear ring of the fourth gear 4) Sleeve of the third and fourth gear 5) Gear ring of the third gear 6) The third gear on the output shaft 7) The second gear on the output shaft 8) Gear ring of the second gear 9) Sleeve of the first and second gear 10) Gear ring of the first gear 11) The first gear on the output shaft 12) Output shaft of the transmission 13) Splined hub 14) Countershaft 15) The first gear on the countershaft 16) The second gear on the countershaft 17) The third gear on the countershaft 18) The constant gear on the countershaft 19) The rotor of the drive motor

3.1. Motion Driven by Drive Motor

The main motion driven by the drive motor corresponds to the synchronization process. According to a previous study in [16], the dynamic model of the synchronization process can be formulated a follows:

$$\begin{bmatrix} \Delta\dot{\theta}_{gr\_slv} \\ \Delta\dot{\omega}_{gr\_slv} \end{bmatrix} = \begin{bmatrix} \Delta\omega_{gr\_slv} \\ \frac{1}{i_g}\frac{T_m - T_{fo}}{J_{in}} \end{bmatrix} \quad \text{Eq. (1)}$$

where $\Delta\theta_{gr-slv}$ and $\Delta\omega_{gr-slv}$ denote the rotational angle difference and speed difference between the gear ring and the sleeve, respectively; i_g is the target gear ratio; T_m and T_{fo} represent the drive motor torque and the disturbance torque from the lubricant oil in the transmission, respectively; and J_{in} is the equivalent inertia of all mechanics connected to the input shaft of the transmission.

3.2. Motion Driven by Shift Motor

During the gear-shifting process, the rotational motion model can be expressed as

$$\begin{bmatrix} \dot{\theta}_a \\ \dot{\omega}_a \end{bmatrix} = \begin{bmatrix} 0 & 1 \\ 0 & -\frac{\zeta_e^a}{J_e^a} \end{bmatrix} \begin{bmatrix} \theta_a \\ \omega_a \end{bmatrix} + \begin{bmatrix} 0 \\ \frac{1}{J_e^a} \end{bmatrix} T_a \quad \text{Eq. (2)}$$

where θ_a and ω_a are the angle and speed of the motor, respectively; ζ_e^a and J_e^a denote the equivalent viscous coefficient and the equivalent inertia of the gear-shifting actuator system, respectively; and T_a represents the torque of the shift motor.

4. Control Strategy

The traditional gear-shifting processes can be divided into five stages, namely, (1) unload, (2) disengagement, (3) synchronization, (4) engagement, and (5) upload. Unload, synchronization, and upload are the actions performed by the drive motor. Synchronization is performed to synchronize the rotational speed and angle between the sleeve and the gear ring. Disengagement and engagement are the actions performed by the shift motor. Figure 2 illustrates the position relations between the sleeve and the gear ring during the gear-shifting process. As depicted, the synchronization process can be started after the sleeve arrives at p_1. The sleeve can successfully engage with the target gear ring without impacts, provided that the synchronization occurs before the sleeve arrives at p_2. To reduce the gear-shifting time, the synchronization driven by the drive motor and the motion flying from p_1 to p_2 driven by the shift motor should be performed simultaneously (Figure 3 depicts the coordination motion relationship). Hence, a time-optimal coordination control strategy is proposed herein.

FIGURE 2 The position relationships between the sleeve and the gear rings.

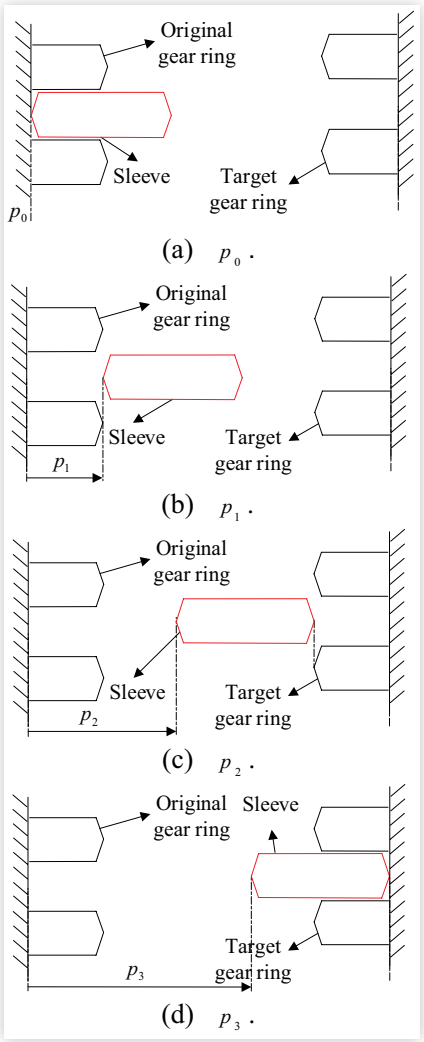

To achieve the time-optimal coordination control policy, the time-optimal dual synchronization control for the drive motor and the time-optimal control for the shift motor are first solved. The time-optimal control for the shift motor is resolved as a bang-off-bang control based on PMP as depicted in Figure 4. For the time of dual synchronization, the time-optimal coordination motion is categorized into two classes. First, if the shift motor with bang-off-bang control drives the sleeve to p_2 after the dual synchronization occurs, the dual synchronization can be coordinated with the shift motor directly with the bang-off-bang control. Details regarding the coordination motion are presented in Section 4.3.1. However, if the sleeve is driven to p_2 before the

FIGURE 3 Gear-shifting motion scheme

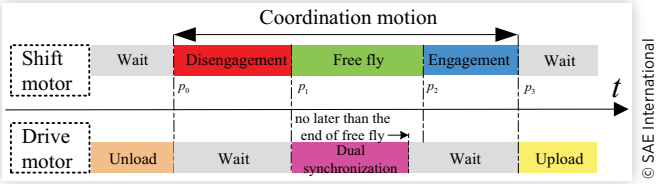

dual synchronization occurs, then the bang-off-bang control cannot be utilized; otherwise, the impacts would occur. In such a case, the sleeve should arrive at p_2 gradually at the same time as that of dual synchronization. Meanwhile, to complete the traversal from p_2 to p_3 with the shortest time after the dual synchronization, the shift motor must operate at the maximum speed. Therefore, an RHC is solved. With the RHC, the rotational speed first decreases and then increases up to the target speed. Meanwhile, the rotational angle reaches the target angle, as depicted in Figure 4. Details regarding the RHC derivation are presented in Section 4.3.2. Finally, a switched time-optimal control between bang-off-bang control and RHC is proposed.

4.1. Time-Optimal Dual Synchronization

Details regarding the time-optimal dual synchronization control are available in a previous study [16]. Therefore, only

FIGURE 4 Two coordination control schemes in the phase plane. The line in red, green, and blue represents the disengagement, the free-fly motion, and the engagement, respectively.

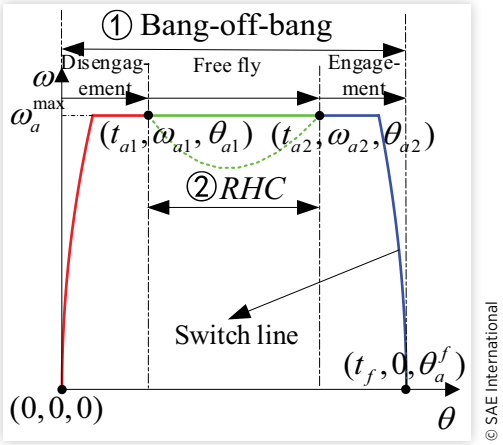

a summary of the time-optimal dual synchronization control is presented herein. As reported in the previous study, the time-optimal dual synchronization control is a bang-bang control, expressed as follows:

$$T_{cmd}^{*}=\begin{cases}-sign\left(\Delta\theta_{gr\_slv}^{*}+\dfrac{\Delta\omega_{gr\_slv}}{2a_{\min}}\right), & \Delta\omega_{gr\_slv}\geq 0\\ -sign\left(\Delta\theta_{gr\_slv}^{*}-\dfrac{\Delta\omega_{gr\_slv}}{2a_{\max}}\right), & \Delta\omega_{gr\_slv}<0\end{cases} \quad \text{Eq. (3)}$$

where $a_{\min}=\left(T_m^{\max}+T_{fo}\right)/J_e$, $a_{\max}=\left(T_m^{\max}-T_{fo}\right)/J_e$ (The oil disturbance is disregarded herein, then $a_{\min}=a_{\max}=T_m^{\max}/J_e$), and $\Delta\theta_{gr\_slv}^{*}$ is the angle difference with an optimal initial angle difference $\Delta\theta_{gr\_slv}^{0*}$.

Previously, the optimal initial angle difference, $\Delta\theta_{gr\_slv}^{0*}$ was solved in [16]. The angle difference varies periodically during the synchronization, which complicates the solving of the optimal control law. To resolve this difficulty, an optimal initial angle difference is proposed, which determines the final relative position of the sleeve and the gear ring with the optimal control law, and is defined as follows:

$$\Delta\theta_{gr\_slv}^{0*}=-\int_0^{t_f}\int_0^{t_f}\frac{T_{cmd}^{*}-T_{fo}}{J_e}dtdt \quad \text{Eq. (4)}$$

where T_{cmd}^{*} is the time-optimal control law during the synchronization process.

Figure 5 depicts the relationship between the real angle difference and the optimal angle differences. As shown, the optimal angle difference is no longer a periodically varied variable. Additionally, the optimal and real angle differences converge to zero simultaneously.

$\Delta\theta_{gr\_slv}^{0*}$ can be calculated as follows:

$$\Delta\theta_{gr\_slv}^{0*}=\begin{cases}\Delta\theta_{gr\_slv}^{0r*}, & t_{fr}\leq t_{fl}\\ \Delta\theta_{gr\_slv}^{0l*}, & t_{fl}<t_{fr}\end{cases} \quad \text{Eq. (5)}$$

where $t_{fr}=\dfrac{\omega_0}{a_{\min}}+\dfrac{\left(a_{\max}+a_{\min}\right)\sqrt{2a_{\min}\Delta\theta_{gr\_slv}^{0r*}+\omega_0^{\,2}}}{a_{\min}\sqrt{a_{\max}\left(a_{\max}+a_{\min}\right)}}$,

$$t_{fl}=-\frac{\omega_0}{a_{\max}}+\frac{\left(a_{\max}+a_{\min}\right)\sqrt{-2a_{\max}\Delta\theta_{gr\_slv}^{0l*}+\omega_0^{\,2}}}{a_{\max}\sqrt{a_{\min}\left(a_{\max}+a_{\min}\right)}}.$$

FIGURE 5 Relationship between the real and optimal angle differences.

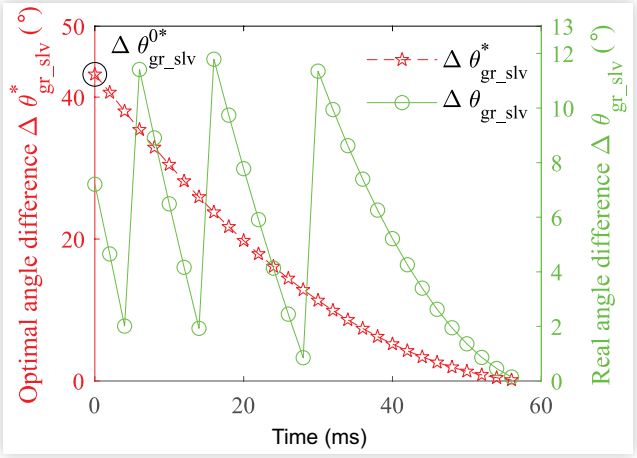

Meanwhile, $\Delta\theta_{gr\_slv}^{0r*}$ can be solved as follows:

1. When $\omega_0\geq 0$,

$$\Delta\theta_{gr\_slv}^{0r*}=\begin{cases}\Delta\theta_{gr\_slv}^{0}-\dfrac{2\pi}{N_{gr}}-K_{\theta}^{1*}\cdot\dfrac{2\pi}{N_{gr}}, & h_1\geq 0\\ \Delta\theta_{gr\_slv}^{0}-K_{\theta}^{1*}\cdot\dfrac{2\pi}{N_{gr}}, & others\end{cases}$$

2. When $\omega_0<0$,

$$\Delta\theta_{gr\_slv}^{0r*}=\begin{cases}\Delta\theta_{gr\_slv}^{0}+K_{\theta}^{4*}\cdot\dfrac{2\pi}{N_{gr}}, & h_2\geq 0\\ \Delta\theta_{gr\_slv}^{0}+\dfrac{2\pi}{N_{gr}}+K_{\theta}^{4*}\cdot\dfrac{2\pi}{N_{gr}}, & others\end{cases}$$

where $K_{\theta}^{i*}=floor\left(\dfrac{\Delta\theta_{gr\_slv}^{i*}}{\dfrac{2\pi}{N_{gr}}}\right)$, $\Delta\theta_{gr\_slv}^{1*}=\dfrac{\omega_0^{\,2}}{2a_{\min}}$,

$$h_1=\Delta\theta_{gr\_slv}^{0}-\frac{2\pi}{N_{gr}}+\mathrm{mod}\left(\Delta\theta_{gr\_slv}^{1*},\frac{2\pi}{N_{gr}}\right),$$

$$\Delta\theta_{gr\_slv}^{4*}=\frac{\omega_0^{\,2}}{2a_{\max}},\ h_2=\Delta\theta_{gr\_slv}^{0}-\mathrm{mod}\left(\Delta\theta_{gr\_slv}^{4*},\frac{2\pi}{N_{gr}}\right).$$

Furthermore, $\Delta\theta_{gr\_slv}^{0l*}$ can be solved as follows:

1. When $\omega_0 \geq 0$,

$$\Delta\theta_{gr\_slv}^{0l*} = \begin{cases} \Delta\theta_{gr\_slv}^{0} - \frac{2\pi}{N_{gr}} - K_{\theta}^{2*} \cdot \frac{2\pi}{N_{gr}}, & h_1 \leq 0 \\ \Delta\theta_{gr\_slv}^{0} - \frac{4\pi}{N_{gr}} - K_{\theta}^{2*} \cdot \frac{2\pi}{N_{gr}}, & others \end{cases}$$

2. When $\omega_0 < 0$,

$$\Delta\theta_{gr\_slv}^{0l*} = \begin{cases} \Delta\theta_{gr\_slv}^{0} + K_{\theta}^{3*} \cdot \frac{2\pi}{N_{gr}}, & h_2 \leq 0 \\ \Delta\theta_{gr\_slv}^{0} - \frac{2\pi}{N_{gr}} + K_{\theta}^{3*} \cdot \frac{2\pi}{N_{gr}}, & others \end{cases}$$

where $\Delta\theta_{gr\_slv}^{2*} = \frac{\omega_0^2}{2a_{\min}}$ and $\Delta\theta_{gr\_slv}^{3*} = \frac{\omega_0^2}{2a_{\max}}$.

4.2. Time-Optimal Motion Control Driven by Shift Motor

During gear shifting the sleeve is driven by the shift motor from p_0 to p_3 in the shortest time such that the problem becomes a fixed terminal time-optimal control problem, as presented in Table 1.

The Hamiltonian function is expressed as:

$$H = 1 + \frac{\lambda_2}{J_e^a} T_a + \left(\lambda_1 - \frac{\zeta_e^a}{J_e^a}\lambda_2\right)\omega_a \qquad \text{Eq. (6)}$$

and the PMP necessary conditions of optimality are as follows:

TABLE 1 Time-optimal control problem statement.

Minimize	$J = \int_0^{t_f} 1dt$
Subject to	*Initial condition*: $\begin{cases}\theta_a^0 = 0 \\ \omega_a^0 = 0\end{cases}$
	Process constraints: Satisfy the constraint of Equation (2) $T_a \in \left[-T_a^{\max}, T_a^{\max}\right]$ $\omega_a \in \left[-\omega_a^{\max}, \omega_a^{\max}\right]$
	Terminal condition: $\begin{cases}\theta_a^f = \theta_{a3} \\ \omega_a^f = 0\end{cases}$

Extremum condition:

$$T_a^* = \underset{T_a \in \Gamma}{\arg\min} H\left(T_a, \theta_a, \omega_a, \lambda_1, \lambda_2\right)$$

State equations:

$$\begin{bmatrix}\dot{\theta}_a^* \\ \dot{\omega}_a^*\end{bmatrix} = \begin{bmatrix}\frac{\partial H}{\partial \lambda_1}\Big|_{T_a^*} \\ \frac{\partial H}{\partial \lambda_2}\Big|_{T_a^*}\end{bmatrix} = \begin{bmatrix}0 & 1 \\ 0 & -\frac{\zeta_e^a}{J_e^a}\end{bmatrix}\begin{bmatrix}\theta_a^* \\ \omega_a^*\end{bmatrix} + \begin{bmatrix}0 \\ \frac{1}{J_e^a}\end{bmatrix} T_a^*$$

Costate equations:

$$\begin{bmatrix}\dot{\lambda}_1 \\ \dot{\lambda}_2\end{bmatrix} = \begin{bmatrix}-\frac{\partial H}{\partial \theta}\Big|_{T_a^*} \\ -\frac{\partial H}{\partial \omega}\Big|_{T_a^*}\end{bmatrix} = \begin{bmatrix}0 \\ -\lambda_1 + \frac{\zeta_e^a}{J_e^a}\lambda_2\end{bmatrix}$$

Boundary conditions:

$$\begin{bmatrix}\theta_a^*(0) \\ \omega_a^*(0) \\ \theta_a^*(t_f) \\ \omega_a^*(t_f)\end{bmatrix} = \begin{bmatrix}\theta_a^0 \\ \omega_a^0 \\ \theta_a^f \\ \omega_a^f\end{bmatrix} = \begin{bmatrix}0 \\ 0 \\ \theta_{a3} \\ 0\end{bmatrix} \qquad \text{Eq. (7)}$$

where $\Gamma = \Gamma_1 \cup \Gamma_2 \cup \Gamma_3$. The constraints of the shift motor speed are as follows:

$$\Gamma_1 = \left\{T_a \middle| -T_a^{\max} \leq T_a \leq \zeta_e^a \omega_a^{\max}, \omega_a = \omega_a^{\max}\right\},$$

$$\Gamma_2 = \left\{T_a \middle| -\zeta_e^a \omega_a^{\max} \leq T_a \leq T_a^{\max}, \omega_a = -\omega_a^{\max}\right\},$$

$$\Gamma_3 = \left\{T_a \middle| -T_a^{\max} \leq T_a \leq T_a^{\max}, -\omega_a^{\max} < \omega_a < \omega_a^{\max}\right\}.$$

According to the costate equations in Equation (7), the costate variables are calculated as follows:

$$\lambda_1 = C_1;\ \lambda_2 = C_2 e^{\frac{\zeta_e^a}{J_e^a}t} + \frac{C_1 J_e^a}{\zeta_e^a} \qquad \text{Eq. (8)}$$

where both C_1 and C_2 are constants.

The Hamiltonian function is a linear function of the control input (T_a). The optimal control input (T_a^*) should achieve the minimum Hamiltonian function with respect to the extremum condition in Equation (7). Therefore, the shift motor torque only should be the maximum or minimum. More specifically, if $\lambda_2 < 0$, the shift motor torque should be the maximum in set Γ. When $\lambda_2 > 0$, the shift motor torque should be the minimum in set Γ.

FIGURE 6 Coordination motion diagram showing bang-off-bang control.

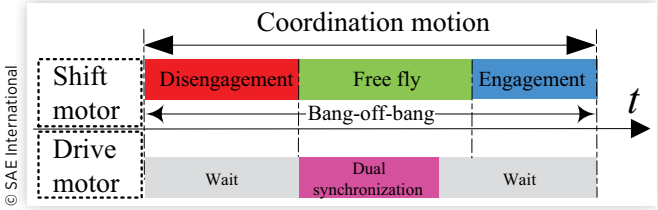

FIGURE 7 Coordination motion diagram showing RHC.

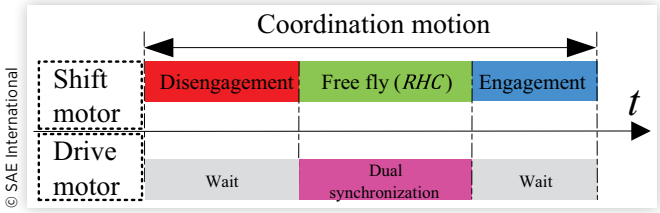

The sign of the torque only changes once at the most as the sign of λ_2 can only change once at the most. For the set Γ, the optimal control should be a bang-off-bang control depicted in Figure 6). The shift motor torque first achieves the maximum torque and accelerates to the maximum. When the shift motor speed is the maximum, the shift motor torque ($T_a = \zeta_e^a \omega_a$) should counteract the viscous resistance torque to maintain the maximum speed. The torque switches to the maximum torque opposite to that in the first stage and drives the shift motor to the desired position when the point in phase plane reaches the switch line depicted in Figure 4. The switch line is calculated as follows (details regarding the derivation of the switch line are provided in Appendix B)

$$\theta_a = \frac{J_e^a\left(\zeta_e^a(-\omega_a) - u^* \log\left[\frac{u^* - \zeta_e^a \omega_a}{u^*}\right]\right)}{\left(\zeta_e^a\right)^2} + \theta_{a3} \quad \text{Eq. (9)}$$

where $u^* = T_a^{\max}$ or $-T_a^{\max}$ depending on whether the shift motor is accelerated or decelerated. In Figure 4, $u^* = -T_a^{\max}$.

The optimal control law can be summarized as follows:

1. When $\theta_{a3} > 0$

$$T_a^{BOB} = \begin{cases} T_a^{\max}, & \omega_a < \omega_a^{\max} \wedge z_1 \geq 0 \\ \zeta_e^a \omega_a^{\max}, & \omega_a = \omega_a^{\max} \\ -T_a^{\max}, & \omega_a < \omega_a^{\max} \wedge z_1 \leq 0 \end{cases} \quad \text{Eq. (10)}$$

$$\text{where } z_1 = \frac{J_e^a\left(\zeta_e^a(-\omega_a) + T_a^{\max} \log\left[\frac{T_a^{\max} + \zeta_e^a \omega_a}{T_a^{\max}}\right]\right)}{\left(\zeta_e^a\right)^2} + \theta_{a3} - \theta_a.$$

2. When $\theta_{a3} < 0$

$$T_a^{BOB} = \begin{cases} -T_a^{\max}, & \omega_a > -\omega_a^{\max} \wedge z_2 \leq 0 \\ -\zeta_e^a \omega_a^{\max}, & \omega_a = -\omega_a^{\max} \\ T_a^{\max}, & \omega_a > -\omega_a^{\max} \wedge z_2 \geq 0 \end{cases} \quad \text{Eq. (11)}$$

$$\text{where } z_2 = \frac{J_e^a\left(\zeta_e^a(-\omega_a) - T_a^{\max} \log\left[\frac{T_a^{\max} - \zeta_e^a \omega_a}{T_a^{\max}}\right]\right)}{\left(\zeta_e^a\right)^2} + \theta_{a3} - \theta_a.$$

4.3. Time-Optimal Coordination Control

As presented in Section 4, the time-optimal control law for the shift motor can be categorized into two classes during the coordination motion. The first class is with the bang-off-bang control. The second class is with the RHC. The details of the derivation for each class are provided below.

4.3.1. Dual Synchronization with Bang-Off-Bang Control

If the free-fly process requires more time than the dual synchronization process ($t_{dual\_syn} < (t_{a2} - t_{a1})$), then the dual synchronization (presented in Section 4.1) with bang-off-bang control (presented in Section 4.2) is the optimal choice. The coordination control diagram is illustrated in Figure 7. After dual synchronization, the drive motor maintains the synchronization state until the shift motor drives the sleeve to engage with the target gear ring.

4.3.2. Dual Synchronization with RHC

In the case of $t_{dual\_syn} \geq (t_{a2} - t_{a1})$, to conserve energy, the integral of the binary norm of the control input is used as the cost function, as presented in Table 2. The terminal time should be equal to the terminal time of dual synchronization such that the start of engagement (θ_{a2}) occurs when the dual synchronization is completed. Meanwhile, the shift motor should achieve its maximum speed at the end of the RHC (Figure 7 illustrates the coordination motion diagram). Therefore, this is a fixed

TABLE 2 Optimal control problem statement.

Minimize	$J = \frac{1}{2}\int_0^{t_f} r T_a^2 dt$
Subject to	*Initial condition*: $\begin{cases} \theta_a^0 = \theta_{a1} \\ \omega_a^0 = \omega_a^{\max} \end{cases}$
	Process constraints: Satisfy the constraint of Equation (2) $T_a \in \left[-T_a^{\max}, T_a^{\max}\right]$ $\omega_a \in \left[-\omega_a^{max}, \omega_a^{max}\right]$
	Terminal condition: $\begin{cases} \theta_a^f = \theta_{a2} \\ \omega_a^f = \omega_a^{max} \\ t_f = t_{dual\_syn} \end{cases}$

terminal time two-point boundary problem. To solve this problem, we first obtain a general analytical solution according to PMP. Subsequently, an RHC is obtained by continuously replacing the initial states with the latest states.

The Hamiltonian function is expressed as follows:

$$H=\frac{1}{2}rT_a^2+\frac{\lambda_2}{J_e^a}T_a+\left(\lambda_1-\frac{\zeta_e^a}{J_e^a}\lambda_2\right)\omega_a \qquad \text{Eq. (12)}$$

Furthermore, the necessary PMP conditions of optimality are

Extremum condition:

$$T_a^*=\underset{T_a\in\Gamma}{\arg\min}H\left(T_a,\theta_a,\omega_a,\lambda_1,\lambda_2\right)$$

State equations:

Same as the state equations in Equation (7)

Costate equations:

$$\begin{bmatrix}\dot{\lambda}_1\\ \dot{\lambda}_2\end{bmatrix}=\begin{bmatrix}-\frac{\partial H}{\partial\theta}\Big|_{T_a^*}\\ -\frac{\partial H}{\partial\omega}\Big|_{T_a^*}\end{bmatrix}=\begin{bmatrix}0\\ -\lambda_1+\frac{\zeta_e^a}{J_e^a}\lambda_2\end{bmatrix}$$

Boundary conditions:

$$\begin{bmatrix}\theta_a^*(0)\\ \omega_a^*(0)\\ \theta_a^*\left(t_{dual\_syn}\right)\\ \omega_a^*\left(t_{dual\_syn}\right)\end{bmatrix}=\begin{bmatrix}\theta_{a1}\\ \omega_a^{\max}\\ \theta_{a2}\\ 0\end{bmatrix} \qquad \text{Eq. (13)}$$

The costates, λ_1 and λ_2, whose dynamics evolves according to the costate equations in Equation (13), are calculated as follows:

$$\lambda_1=C_1;\quad \lambda_2=C_2e^{\frac{\zeta_e^a}{J_e^a}t}+\frac{C_1J_e^a}{\zeta_e^a} \qquad \text{Eq. (14)}$$

According to the extremum condition, the optimal control law can be solved as follows:

$$\left.\frac{\partial H}{\partial T_a}\right|_{T_a^*}=0\Rightarrow T_a^*=-\frac{\lambda_2}{rJ_e^a} \qquad \text{Eq. (15)}$$

Substituting the shift motor torque of Equation (2) with the result of Equation (15) and integrating the ODEs in Equation (2), the states at a time t can be solved as follows:

$$\begin{bmatrix}\omega_t & \theta_t\end{bmatrix}^T=-\frac{1}{2r\left(\zeta_e^a\right)^2}W\begin{bmatrix}C_1 & C_2 & C_3 & C_4\end{bmatrix}^T \qquad \text{Eq. (16)}$$

where $W=\begin{bmatrix}2 & \frac{\zeta_e^a}{J_e^a}e^{\frac{\zeta_e^a}{J_e^a}t} & -2r\left(\zeta_e^a\right)^2e^{-\frac{\zeta_e^a}{J_e^a}t} & 0\\ 2t & e^{\frac{\zeta_e^a}{J_e^a}t} & 2rJ_e^a\zeta_e^ae^{-\frac{\zeta_e^a}{J_e^a}t} & -2r\left(\zeta_e^a\right)^2\end{bmatrix}$.

Subsequently, the boundary conditions shown in Equation (13) can be rewritten as follows:

$$\begin{bmatrix}\omega_a^0 & \theta_a^0 & \omega_a^f & \theta_a^f\end{bmatrix}^T=-\frac{1}{2r\left(\zeta_e^a\right)^2}M\begin{bmatrix}C_1 & C_2 & C_3 & C_4\end{bmatrix}^T \qquad \text{Eq. (17)}$$

where $M=\begin{bmatrix}2 & \frac{\zeta_e^a}{J_e^a} & -2r\left(\zeta_e^a\right)^2 & 0\\ 0 & 1 & 2rJ_e^a\zeta_e^a & -2r\left(\zeta_e^a\right)^2\\ 2 & \frac{\zeta_e^ae^{\frac{\zeta_e^a}{J_e^a}t_f}}{J_e^a} & -2r\left(\zeta_e^a\right)^2e^{-\frac{\zeta_e^a}{J_e^a}t_f} & 0\\ 2t_f & e^{\frac{\zeta_e^a}{J_e^a}t_f} & 2rJ_e^a\zeta_e^ae^{-\frac{\zeta_e^a}{J_e^a}t_f} & -2r\left(\zeta_e^a\right)^2\end{bmatrix}$.

It can be proven that the square matrix (M) on the right is invertible (full rank). The details of the proof are presented in Appendix C.

Based on Equations (14), (15), and (17), the optimal control input can be calculated as follows:

$$T_a^*=2\left(\zeta_e^a\right)^2\begin{bmatrix}\frac{1}{\zeta_e^a} & \frac{e^{\frac{\zeta_e^a}{J_e^a}t}}{J_e^a} & 0 & 0\end{bmatrix}M^{-1}\begin{bmatrix}\omega_a^0 & \theta_a^0 & \omega_a^f & \theta_a^f\end{bmatrix}^T \qquad \text{Eq. (18)}$$

As time progresses, the initial states are substituted by the latest states. The corresponding control input uses the first value; this implies that $t=0,\omega_a^0=\omega_a^{cur}$, and $\theta_a^0=\theta_a^{cur}$ in Equation (18). The RHC is obtained as follows:

$$T_a^{RHC}=2\left(\zeta_e^a\right)^2VM^{-1}\Omega \qquad \text{Eq. (19)}$$

where $V=\left[\frac{1}{\zeta_e^a},\frac{1}{J_e^a},0,0\right]$ and $\Omega=\left[\omega_a^{cur},\theta_a^{cur},\omega_a^f,\theta_a^f\right]^T$.

5. Results and Analysis

Figure 8 illustrates the flow-chart of the control scheme. Based on the flow-chart, two cases are first presented in the following with bang-off-bang control or RHC using the parameters listed in Table 3. The simulation step size is 100 μs. Subsequently, the method to find appropriate parameters of the drive motor and the shift motor are analyzed based on the control strategy.

5.1. Case Study with Bang-Off-Bang Control

Figure 9 illustrates an example of the coordination motion with dual synchronization and bang-off-bang control. At the

FIGURE 8 Flowchart of the coordination control.

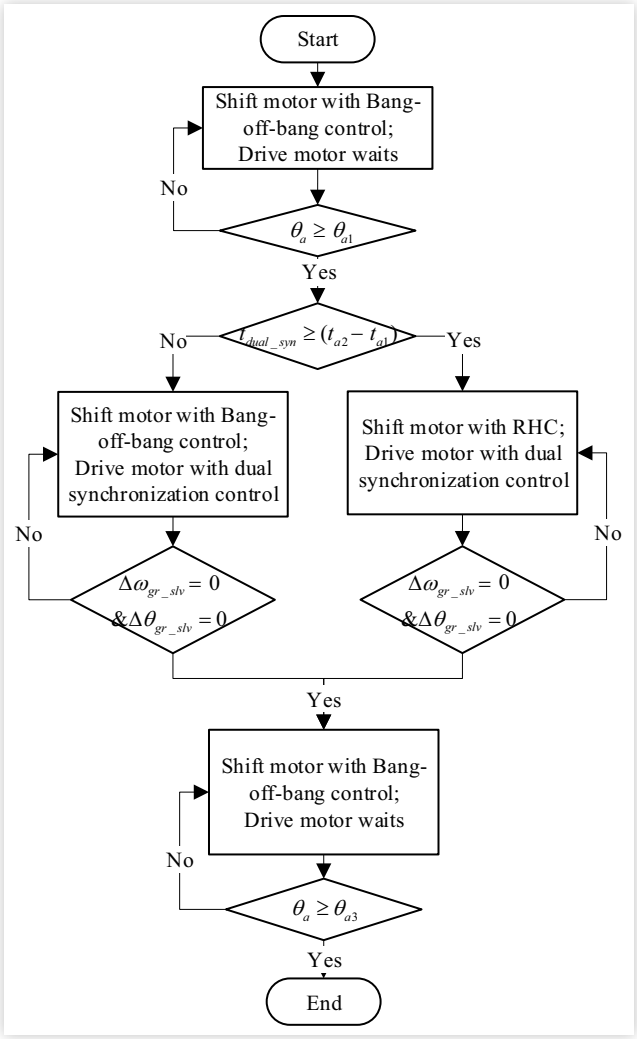

disengagement phase, the shift motor is first driven to the maximum speed with the maximum torque. Subsequently, the shift motor maintains the maximum speed by balancing the viscous resistance with a small torque. After the disengagement, the dual synchronization and free-fly processes start simultaneously. The shift motor maintains its maximum speed at this stage. The dual synchronization ends before the free-fly process. Subsequently, the shift motor launches to the switch line with maximum speed and then decelerates to zero with the maximum torque, while the drive motor maintains the dual synchronization.

5.2. Case Study with RHC

Figure 10 depicts the coordination motion of dual synchronization with RHC. As shown, the dual synchronization and free-fly process occur simultaneously with the same start and end time points. During the coordination motion, the shift motor speed first decreases and then recovers to the maximum speed to complete the remaining process in the shortest time.

TABLE 3 Transmission parameters.

Parameters	Value	Unit
Maximum drive motor torque (T_m^{max})	400	Nm
Initial speed difference ($\omega_{gr\_slv}^0, \omega_0$)	-209.47 (bang-off-bang), -310 (RHC)	rpm
Equivalent inertia (J_e)	1.0025	kgm/s^2
Teeth number of sleeve (N_{gr})	30	-
Transmission ratio (i_g)	4.01	-
Maximum shift motor torque (T_a^{max})	0.8	Nm
Equivalent viscous coefficient (ζ_e^a)	1.5×10^{-4}	Nm/(rad/s)
Equivalent inertia (J_e^a)	2.49×10^{-5}	kgm/s^2
p_1	6.75	mm
p_2	20.25	mm
p_3	27	mm
r_f	48	mm
i_r	68/24	-
i_r	20	-

5.3. Optimal Parameters Match between Shift Motor and Drive Motor

The free-fly process time of the shift motor and the dual synchronization process time of the drive motor should match. The free-fly process time depends on the maximum speed, which can be solved as follows:

$$t_{free} = \frac{\theta_{a2} - \theta_{a1}}{\omega_a^{max}} \qquad \text{Eq. (20)}$$

The dual synchronization time is mainly dependent on the initial speed difference, according to a previous study [16]. The optimal dual synchronization time can be calculated approximately as follows:

$$t_{dual\_syn} = \frac{|\omega_0|}{T_m^{\max} / J_e} + (0 \sim C_{time}) \qquad \text{Eq. (21)}$$

where C_{time} is the maximum time difference between the optimal dual synchronization and the pure speed synchronization, i.e., approximately 0.015 s.

It is clear that the free-fly time should be within the dual synchronization time. That implies that $\max(t_{dual\_syn}) \geq t_{free} \geq \min(t_{dual\_syn})$, whose simplicity form is shown in Equation (22). As shown, the initial speed difference is negatively correlated to the maximum shift motor speed. Therefore, Equation (22) should be considered when designing parameters.

$$\frac{|\omega_0|}{T_m^{\max} / J_e} \leq \frac{\theta_2 - \theta_1}{\omega_a^{\max}} \leq \frac{|\omega_0|}{T_m^{\max} / J_e} + C_{time} \qquad \text{Eq. (22)}$$

FIGURE 9 Results of bang-off-bang control.

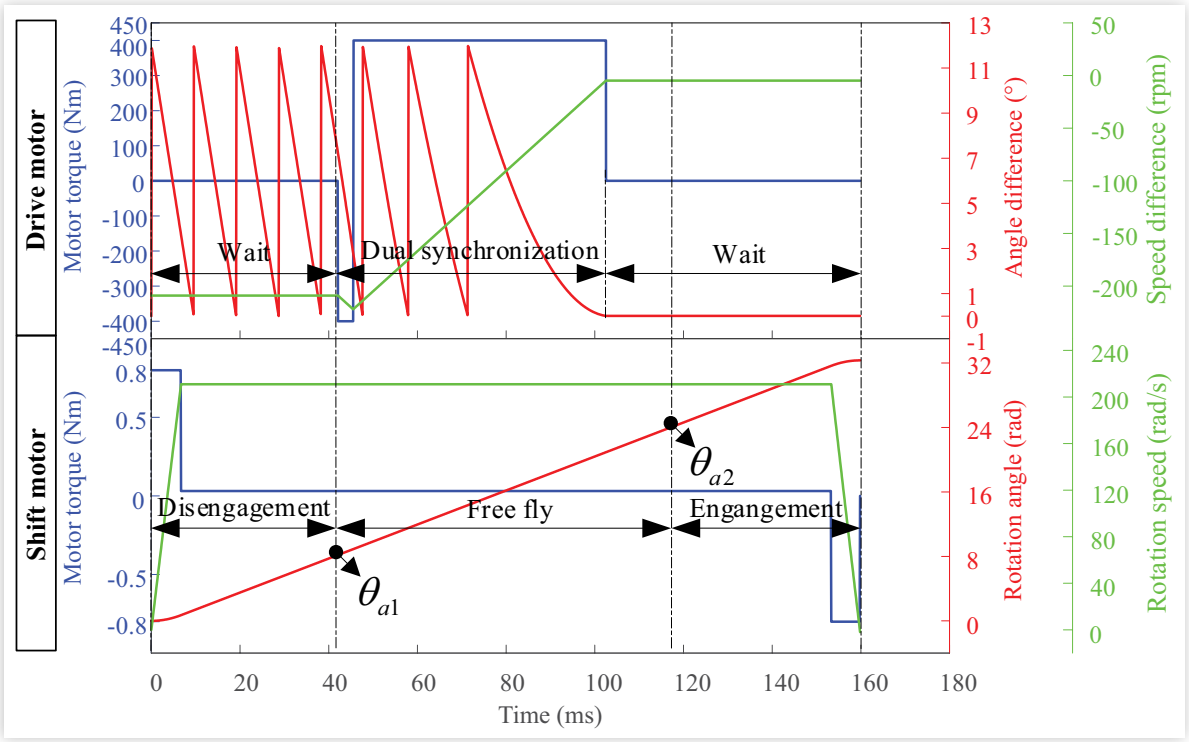

FIGURE 10 Results of RHC.

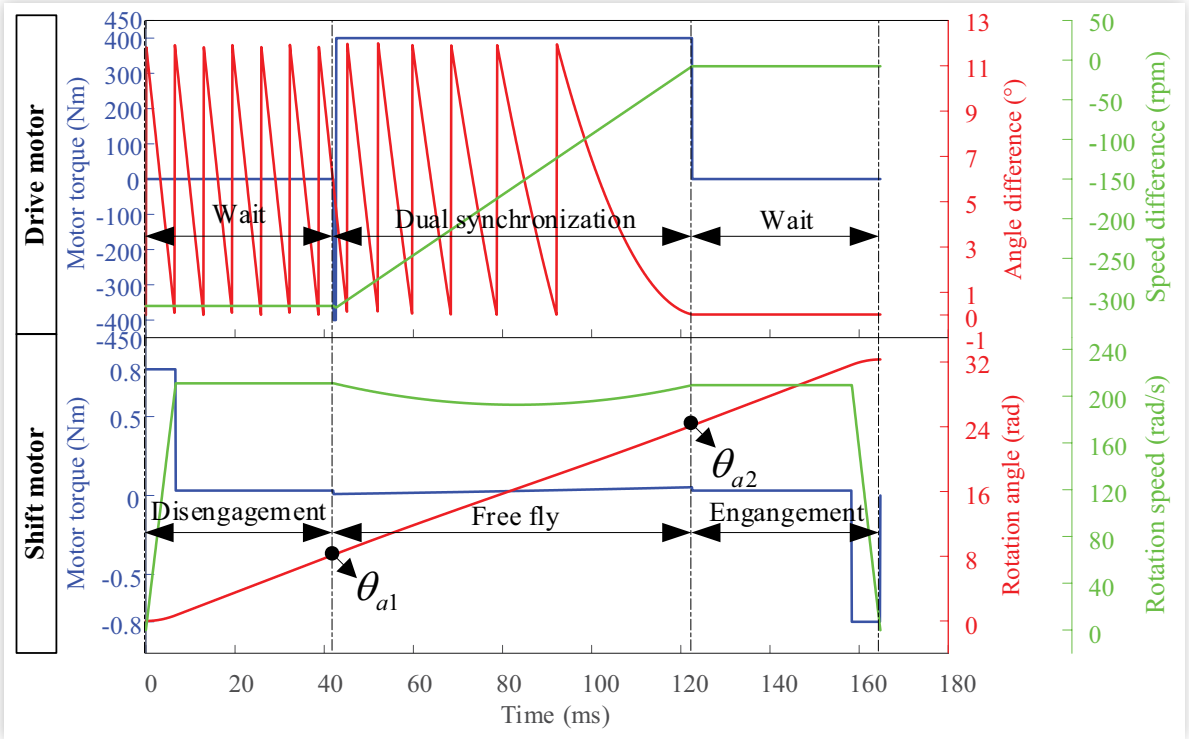

6. Conclusion

Herein, a time-optimal coordination control between the dual synchronization of a drive motor and the position control of a shift motor is proposed. The time-optimal dual synchronization control in a previous study [16] was first reviewed. The time-optimal position control of the shift motor was solved based on the PMP. Based on an analysis, the time-optimal coordination control can be categorized into two classes.

1. When the dual synchronization process is terminated before the sleeve arrives at the start of engagement with bang-off-bang control, the bang-off-bang control is applied to drive the shift motor.
2. When the dual synchronization process is completed after the sleeve arrives at the start of engagement with bang-off-bang control, an RHC law is obtained by solving a fixed terminal time two-point boundary values problem. The RHC is proposed to arrive at the start of engagement with the same time cost as that of the dual synchronization.

Moreover, the optimal parameters' relationship between the drive motor and the shift motor was obtained through analysis. According to the relationship, the initial speed difference is negatively correlated with the maximum shift motor speed. Furthermore, the relationship provides a reference for the design of the maximum torque of the drive motor, the inertia of the transmission, and the maximum speed of the shift motor.

The proposed theoretical time-optimal coordination control can be used as a forward control. It can be easily implemented by calculating the necessary matrices in advance as the system parameters are constant.

Future studies include the design of a feedback control to improve the anti-disturbance performance of the system, followed by the verification of the strategy on a test bench.

Contact Information

Corresponding author:
Ziwang Lu
luzw1992@gmail.com

Acknowledgment

We would like to acknowledge the funding support of the National Natural Science Foundation of China (Grant No. 51775291) and the China Scholarship Council (201806210156).

List of Symbols

Symbol list related to the drive motor

T_m^{max} - The maximum torque of the drive motor

T_{cmd} - Torque command for the drive motor

T_0, T_E - The drive motor torque at the start point and the end point of the transient process

T_{fo} - The disturbance torque from the lubricant oil in the transmission

$\Delta\theta_{gr\_slv}$ - Angle difference between the target gear ring and the sleeve

ω_0 - Initial speed difference between the target gear ring and the sleeve

N_{gr} - Number of teeth on the target gear ring or sleeve

i_g - Transmission ratio for the target gear

J_{in} - Equivalent inertia on the input shaft including all mechanisms connected to the input shaft of the transmission

J_e - Equivalent inertia on the target gear ring, which can be derived from J_{in}, $J_e = J_{in} i_g$

t_{dual_syn} - Time for the dual synchronization

Symbol list related to gear-shifting actuator

T_a - Torque out of the shift motor

T_a^{max} - The maximum torque of the shift motor

θ_a - Angle of the shift motor

θ_a^0 - Angle of the shift motor at the start of the gear-shifting process

θ_{a1} - Angle of the shift motor at the end of disengagement

θ_{a2} - Angle of the shift motor at the start of engagement

θ_a^f, θ_{a3} - Angle of the shift motor at the end of the gear-shifting process

θ_a^{cur} - The latest angle of the shift motor

ω_a - Speed of the shift motor

ω_a^{max} - The maximum speed of the shift motor

ω_a^0 - Speed of the shift motor at the start of the gear-shifting process

ω_{a1} - Speed of the shift motor at the end of disengagement

ω_{a2} - Speed of the shift motor at the start of the engagement

ω_a^f - Speed of the shift motor at the end of the gear-shifting process

ω_a^{cur} - The latest speed of the shift motor

ζ_e^a - Equivalent viscous coefficient of the gear-shifting actuator system

J_e^a - Equivalent inertia of the gear-shifting actuator system

t_{a1} - Time for the motion from the start of the gear-shifting process to the end of disengagement

t_{a2} - Time for the motion from the start of the gear-shifting process to the start of engagement

t_{free} - Time for the motion from the end of disengagement to the start of engagement ($t_{free} = t_{a2} - t_{a1}$).

References

1. Barton, B. and Schütte, P., "Electric Vehicle Law and Policy: A Comparative Analysis," *Journal of Energy & Natural Resources Law* 35:147-170, 2017.

2. Ren, Q., Crolla, D.A., and Morris, A., "Effect of Transmission Design on Electric Vehicle (EV) Performance," in *5th IEEE Vehicle Power and Propulsion Conference, VPPC '09*, Dearborn, MI, 2009, 1260-1265, https://doi.org/10.1109/VPPC.2009.5289707.
3. Hofman, T. and Dai, C.H., "Energy Efficiency Analysis and Comparison of Transmission Technologies for an Electric Vehicle," in *2010 IEEE Vehicle Power and Propulsion Conference, VPPC 2010*, Lille, Northern France, 2010, 1-6, https://doi.org/10.1109/VPPC.2010.5729082.
4. Falcone, F., Burns, J., and Nelson, D., "Closed Loop Transaxle Synchronization Control Design," SAE Technical Paper 2010-01-0817, 2010, https://doi.org/10.4271/2010-01-0817.
5. Yu, H.-L., Xi, J.-Q., Zhang, F. et al., "Research on Gear Shifting Process without Disengaging Clutch for a Parallel Hybrid Electric Vehicle Equipped with AMT," *Mathematical Problems in Engineering* 2014:1-12, 2014.
6. Fu, H., Tian, G., Chen, Y., et al., "A Novel Control Scheme of Propulsion Motor for Integrated Powertrain of Electric Bus," in *2009 IEEE Vehicle Power and Propulsion Conference*, Dearborn, MI, 2009, 1496-1501.
7. Yu, C.-H., Tseng, C.-Y., and Wang, C.-P., "Smooth Gear-Change Control for EV Clutchless Automatic Manual Transmission," in *2012 IEEE/ASME International Conference on Advanced Intelligent Mechatronics (AIM)*, Kaohsiung, Taiwan, 2012, 971-976.
8. Tseng, C.-Y. and Yu, C.-H., "Advanced Shifting Control of Synchronizer Mechanisms for Clutchless Automatic Manual Transmission in an Electric Vehicle," *Mechanism and Machine Theory* 84:37-56, 2015.
9. Zhu, X., Zhang, H., Xi, J. et al., "Robust Speed Synchronization Control for Clutchless Automated Manual Transmission Systems in Electric Vehicles," *Proceedings of the Institution of Mechanical Engineers, Part D: Journal of Automobile Engineering* 229:424-436, 2015, https://doi.org/10.1177/0954407014546431.
10. Breen, J. and Bower, G., "Clutchless Shifting of an Automated Manual Transmission in a Hybrid Powertrain," SAE Technical Paper 2011-01-2194, 2011, https://doi.org/10.4271/2011-01-2194.
11. Dong, X.Y., Xi, J.Q., and Chen, H.Y., "The Power System Active-Synchronizing Control of the PHEV during the AMT Shifting Process," *Applied Mechanics and Materials* 1155-1159, 2011.
12. Yan, T., Yang, L., Yan, B. et al., "Dynamic Shift Coordinated Control Based on Motor Active Speed Synchronization with the New Hybrid System," *Shock and Vibration* 2017:1-16, 2017.
13. Bóka, G., Lovas, L., Márialigeti, J. et al., "Engagement Capability of Face-Dog Clutches on Heavy Duty Automated Mechanical Transmissions with Transmission Brake," *Proceedings of the Institution of Mechanical Engineers, Part D: Journal of Automobile Engineering* 224:1125-1139, 2010, https://doi.org/10.1243/09544070JAUTO1435.
14. Lei, Y., Hu, J., Fu, Y. et al., "Control Strategy of Automated Manual Transmission Based on Active Synchronisation of Driving Motor in Electric Bus," *Advances in Mechanical Engineering* 11:1-17, 2019, https://doi.org/10.1177/1687814019846734.
15. Piracha, M., Grauers, A., Barrientos, E., Budacs, H. et al., "Model Based Control of Synchronizers for Reducing Impacts during Sleeve to Gear Engagement," SAE Technical Paper 2019-01-1303, 2019, https://doi.org/10.4271/2019-01-1303.
16. Lu, Z., Chen, H., Wang, L., et al., "Optimal Dual Synchronization Control of Rotational Speed and Angle in Non-synchronizer Automatic Mechanical Transmission," 2018. https://www.researchgate.net/publication/336654128_Optimal_Dual_Synchronization_Control_of_Rotational_Speed_and_Angle_in_Non-synchronizer_Automatic_Mechanical_Transmission, accessed February 19, 2020.
17. Kumbhar, M.S. and Panchagade, D.R., "A Literature Review on Automated Manual Transmission (AMT)," *Int J Sci Res Dev* 2:1236-1239, 2014.
18. Zhong, Z., Kong, G., Yu, Z. et al., "Concept Evaluation of a Novel Gear Selector for Automated Manual Transmissions," *Mechanical Systems and Signal Processing* 31:316-331, 2012.
19. Zhong, Z., Kong, G., Yu, Z. et al., "Shifting Control of an Automated Mechanical Transmission without Using the Clutch," *International Journal of Automotive Technology* 13:487-496, 2012.
20. Gao, Z., Zhong, Z., and Sun, Z., "Optimal Position Control for Motor-Driven Shifting Actuator in Electrical AMT," *Automot Eng* 33:133-137, 2011.
21. Chen, Z., Zhang, B., Zhang, N. et al., "Optimal Preview Position Control for Shifting Actuators of Automated Manual Transmission," *Proceedings of the Institution of Mechanical Engineers, Part D: Journal of Automobile Engineering* 233:440-452, 2019.

Appendix A: Gear-Shifting Actuator Geometry

Figure A.1 illustrates the geometry of the gear-shifting actuator. The gear-shifting actuator converts the electric power of the motor to the mechanical power of the sleeve through a planetary reducer, a gear reducer, and the contact between the shift finger and the sleeve. Meanwhile, the rotational motion of the drive motor is converted to the translational motion of the sleeve. The power flow is indicated in red. For the geometry shown, the specific positions of the shift finger and the shift motor can be solved according to the following equations.

1. Rotational angle of the shift finger

$$\theta^3_{finger} = 2\arcsin\left(\frac{p_3}{2r_f}\right);\quad \theta^2_{finger} = \frac{\theta^3_{finger}}{2} + \arcsin\left(\frac{p_2 - \frac{p_3}{2}}{r_f}\right);$$
$$\theta^1_{finger} = \frac{\theta^3_{finger}}{2} - \arcsin\left(\frac{\frac{p_3}{2} - p_1}{r_f}\right) \qquad \text{Eq. (A.1)}$$

2. Rotational angle of the shift motor

$$\theta_{a3} = i_p i_r \theta^3_{finger};\quad \theta_{a2} = i_p i_r \theta^2_{finger};\quad \theta_{a1} = i_p i_r \theta^1_{finger} \qquad \text{Eq. (A.2)}$$

FIGURE A.1 Mechanical scheme of the gear-shifting actuator.

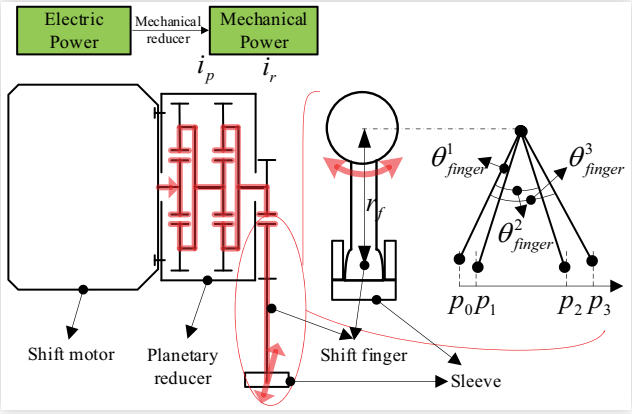

Appendix B: Solution of Switch Line

The first-order derivative of the shift motor speed can be calculated as follows:

$$\dot{\omega}_a = -\frac{\zeta^a_e}{J^a_e}\omega_a + \frac{1}{J^a_e}u^* \ with\ \omega_a(0) = \omega^0_a \qquad \text{Eq. (B.1)}$$

where $u^* = T^{max}_a$ or $-T^{max}_a$ based on whether it is accelerated or decelerated.

The integral of Equation (B.1) can be solved as follows

$$\omega_a(t) = \frac{\left(1 - e^{-\frac{\zeta^a_e}{J^a_e}t}\right)u^*}{\zeta^a_e} + \omega^0_a e^{-\frac{\zeta^a_e}{J^a_e}t} \qquad \text{Eq. (B.2)}$$

The first-order derivative of the shift motor angle can be calculated as

$$\dot{\theta}_a = \omega_a \ with\ \theta_a(0) = \theta^0_a \qquad \text{Eq. (B.3)}$$

The integral of Equation (B.3) can be solved as

$$\theta_a(t) = \frac{J^a_e\left(\zeta^a_e\omega^0_a\left(1 - e^{-\frac{\zeta^a_e}{J^a_e}t}\right) - u^*\left(1 - e^{-\frac{\zeta^a_e}{J^a_e}t} - \frac{\zeta^a_e}{J^a_e}t\right)\right)}{\left(\zeta^a_e\right)^2} + \theta^0_a \qquad \text{Eq. (B.4)}$$

Substituting the shift motor speed and angle with the speed and angle destination $\left(\omega_a(t^*) = \omega^*_a, \theta_a(t^*) = \theta^*_a\right)$ in Equations (B.2) and (B.4), the equation of the switch lines can be solved as follows:

$$\theta^0_a = \frac{J^a_e\left(\zeta^a_e\left(\omega^*_a - \omega^0_a\right) - u^*\log\left[\frac{u^* - \zeta^a_e\omega^0_a}{u^* - \zeta^a_e\omega^*_a}\right]\right)}{\left(\zeta^a_e\right)^2} + \theta^*_a \qquad \text{Eq. (B.5)}$$

In fact, Equation (B.5) is symmetric. This implies that the states at the end time exhibit the same relationship as that at the start time, i.e., $\theta^*_a = \frac{J^a_e\left(\zeta^a_e\left(\omega^0_a - \omega^*_a\right) - u^*\log\left[\frac{u^* - \zeta^a_e\omega^*_a}{u^* - \zeta^a_e\omega^0_a}\right]\right)}{\left(\zeta^a_e\right)^2} + \theta^0_a$. The switch lines are depicted in Figure B.1.

FIGURE B.1 Switch line in the phase plane.

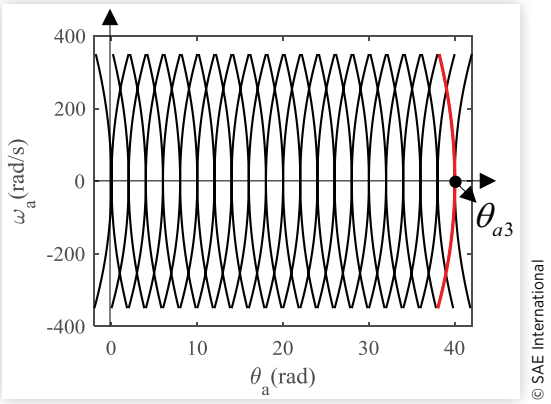

Appendix C: Proof of Matrix (*M*) Invertibility

1. Elementary row transformation

After the elementary row transformation, M can be converted into a block matrix as, i.e., $\begin{bmatrix} A & 0 \\ \cdot & B \end{bmatrix}$. In the block matrix, $A = \begin{bmatrix} A_{11} & A_{12} \\ A_{21} & A_{22} \end{bmatrix}$, $A_{12} = \dfrac{\zeta_e^a e^{-\frac{\zeta_e^a}{J_e^a}t_f}\left(1-e^{\frac{\zeta_e^a}{J_e^a}t_f}\right)\left(1+e^{\frac{\zeta_e^a}{J_e^a}t_f}\right)}{J_e^a}$, $A_{22} = 0$, and $B = \begin{bmatrix} -2r\left(\zeta_e^a\right)^2 e^{-\frac{\zeta_e^a}{J_e^a}t_f} & 0 \\ 2rJ_e^a\zeta_e^a e^{-\frac{\zeta_e^a}{J_e^a}t_f} & -2r\left(\zeta_e^a\right)^2 \end{bmatrix}$. Through matrix inference, $r\left(\begin{bmatrix} A & 0 \\ \cdot & B \end{bmatrix}\right) \le r(A) + r(B)$. Furthermore, it is clear that B is a full rank matrix. Therefore, A must be verified as a full rank matrix.

2. Full rank proof of A
To verify A is a full rank matrix, the determinant of A must be proven to be unequal to zero. Therefore, A_{12} and A_{21} should be unequal to zero. It is clear that A_{12} and the denominator of A_{21}, $\left(e^{\frac{\zeta_e^a}{J_e^a}t_f} - 1\right)$, are equal to zero only when t_f is equal to zero. Next, we must prove that $\left(4+2\dfrac{\zeta_e^a}{J_e^a}t_f\right)\left(1-e^{-\frac{\zeta_e^a}{J_e^a}t_f}\right) - 4\dfrac{\zeta_e^a}{J_e^a}t_f$ is unequal to zero.

3. Nonzero proof
To prove that $\left(4+2\dfrac{\zeta_e^a}{J_e^a}t_f\right)\left(1-e^{-\frac{\zeta_e^a}{J_e^a}t_f}\right) - 4\dfrac{\zeta_e^a}{J_e^a}t_f$ is unequal to zero based on the fact that $\left(e^{\frac{\zeta_e^a}{J_e^a}t_f} - 1\right)$ is unequal to zero, we define a function $f(t_f) = \left(4+2\dfrac{\zeta_e^a}{J_e^a}t_f\right)\left(1-e^{-\frac{\zeta_e^a}{J_e^a}t_f}\right) - 4\dfrac{\zeta_e^a}{J_e^a}t_f$. To simplify the notation, Q is used to substitute $\dfrac{\zeta_e^a}{J_e^a}$. Therefore,

$$\begin{aligned} f(t_f) &= (4+2Qt_f)\left(1-e^{-Qt_f}\right) - 4Qt_f; \\ f'(t_f) &= 2Qe^{-Qt_f}\left(1-e^{Qt_f} + Qt_f\right); \\ f''(t_f) &= -2Q^3e^{-Qt_f}t_f \end{aligned} \qquad \text{Eq. (C.1)}$$

$f''(0) = 0$, $f'(0) = 0$, $f(0) = 0$ and $f''(t_f) < 0$ *with* $t_f > 0$. Therefore, $f'(t_f) < 0$, $f(t_f) < 0$ *with* $t_f > 0$. This implies that $\left(4+2\dfrac{\zeta_e^a}{J_e^a}t_f\right)\left(1-e^{-\frac{\zeta_e^a}{J_e^a}t_f}\right) - 4\dfrac{\zeta_e^a}{J_e^a}t_f$ is equal to zero only if $t_f = 0$.